Materials Chemistry

Cite this: *J. Mater. Chem.*, 2011, **21**, 14849

www.rsc.org/materials

PAPER

Implementing chemical functionality into oriented films of metal–organic frameworks on self-assembled monolayers†

Camilla Scherb,[a] Jennifer J. Williams,[b] Florian Hinterholzinger,[a] Sebastian Bauer,[c] Norbert Stock[c] and Thomas Bein*[a]

Received 25th December 2010, Accepted 10th May 2011
DOI: 10.1039/c0jm04526h

The generation of thin films of oriented functionalized metal–organic frameworks (MOFs) on self-assembled monolayers was achieved *via* direct growth from solution. Specifically, the direct growth from solvothermally pretreated synthesis solutions of two different MOF structures with amino functionality was investigated: the flexible framework structure NH_2–Fe–MIL-88B and the mesoporous MOF NH_2–Fe–MIL-101 with its remarkably large unit cell. Both MOF structures can be grown in a highly oriented fashion on self-assembled monolayers of 16-mercaptohexadecanoic acid on gold. With the help of a quartz crystal microbalance we demonstrate that the introduction of amino groups into the framework strongly affects the host–guest interactions towards ethanol molecules: thin films of NH_2–Fe–MIL-88B show a significantly higher uptake of ethanol than unfunctionalized Fe–MIL-88B films. *In situ* XRD experiments during sorption of ethanol showed that the amino group does have an impact on the cell parameters of the structure, but the flexibility ("breathing") during ad- and desorption of ethanol is similar for the functionalized and the unfunctionalized structures. It is anticipated that the implementation of chemical functionalities into oriented MOF films will lead to selective host–guest interactions that are of key importance for chemical sensing and other applications.

Introduction

Metal–organic frameworks (MOFs), also called coordination polymers, have attracted enormous attention due to their highly modular construction principles based on molecular building blocks. Numerous applications in gas storage, separation techniques, sensing, catalysis, and drug release are envisioned.[1–5] For several of these applications, it would be highly desirable to prepare thin films with oriented channel structures. Several different approaches for the synthesis of MOF thin films have recently been reported, see a review by Zacher *et al.*[6] For example, Shekhah *et al.* developed a step-by-step route, whereby a functionalized substrate is sequentially immersed into alternating solutions of a metal salt and the organic component of the particular structure.[7–9] It was found that the formation of secondary building units (SBUs) is essential for the subsequent crystallization of MOFs.[10] Several MOF-based films have also been made by the direct growth method, where a functionalized substrate is exposed to a pre-treated crystallization solution of a particular MOF.[11–13] The mechanism of direct growth of MOFs on functionalized substrates is proposed to be analogous to the self-assembly process during the formation of MOF crystals. The concept of direct growth of MOF crystals on self-assembled organic monolayers (SAMs) is depicted in Scheme 1.

The central concept is to use the particular functional group of organic linkers in a certain MOF structure as the functional terminal group of the SAM. This enables coordination of the metal ions or SBUs from the solution to the surface. The attached metal centers or SBUs will subsequently be coordinated by the organic ligands present in the solution; this process further leads to the crystal growth of the desired MOF, with the crystals being directly attached to the surface. We have recently reported the first example of tunable, oriented growth of MOFs on different functionalized SAMs for the MOF HKUST-1.[14] This synthetic protocol was also successfully employed for *in situ* AFM investigations of crystal growth of a sub-micron sized HKUST-1 crystal.[15]

Extending the concept of directing the structure and orientation of MOFs using self-assembled monolayers for surface

[a]*Department of Chemistry and Center for NanoScience (CeNS), University of Munich (LMU), Butenandtstr. 11 (Gerhard-Ertl-Building, E), 81377 Munich, Germany; Web: www.cup.uni-muenchen.de/pc/bein; Fax: +49 89218077622; Tel: +49 89218077621*

[b]*Institute for Materials and Processes, School of Engineering, University of Edinburgh, EH9 3JL, UK*

[c]*Department of Inorganic Chemistry, Christian-Albrechts-University of Kiel, Otto-Hahn-Platz, 6/7, 24098 Kiel, Germany*

† Electronic supplementary information (ESI) available: RAIR characterization of self-assembled monolayers, additional information derived from X-ray diffraction and TG and sorption data of bulk NH_2–Fe–MIL-101 as well as reproduced QCM experiments of NH_2–Fe–MIL-88B and its unfunctionalized counterpart. See DOI: 10.1039/c0jm04526h

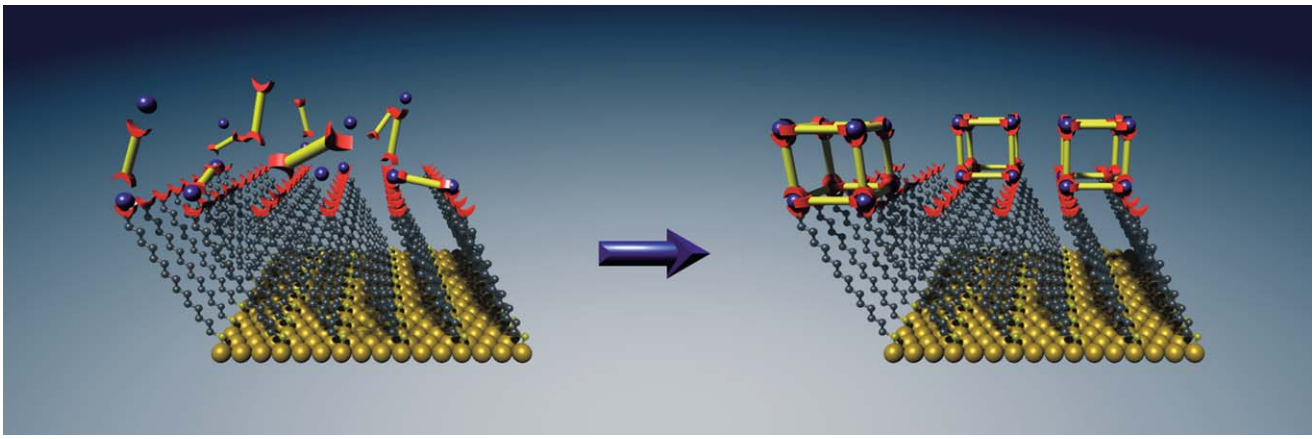

Scheme 1 Concept of direct growth of MOFs on SAM-functionalized gold substrates.

functionalization, we now ask if we can implement chemical functionalities into films of oriented MOF structures. For example, uncoordinated functional groups on the organic ligands could offer tunable interactions with encapsulated species. This could result in more selective materials with a higher capacity in fields such as chemical sensing, gas separation or storage.[16]

There are two different approaches to implementing functionalities in MOFs. The first employs organic ligands with additional functional groups that are not involved in coordination of the metal centers but rather change the functionality of the pore walls. Kitagawa *et al.* have focused their research efforts on this challenge. They modified the organic linkers in such a way that the host–guest interactions desired for a particular application were obtained by inserting unsaturated metal-centres.[17] In a different study, the same group reports the implementation of hydrogen-bonding groups for specific host–guest interactions within dynamic porous coordination polymers.[18] The second approach refers to the post-synthetic modification of the organic linkers, which in most cases requires the presence of at least one modifiable functional group.[19,20] For example, Kim and co-workers showed that the pendant pyridyl groups in a chiral zinc network could be methylated.[21] Burrows *et al.* reported a post-synthetic modification starting from an aldehyde-functionalized dicarboxylate to a hydrazone ligand.[22] In other studies it has been demonstrated that the amino groups in 2-amino-1,4-benzenedicarboxylate MOFs can be converted into amides, urethanes,[23–25] or salicylidenes.[26]

Following the first approach, Bauer *et al.* were able to obtain powders of the amino-functionalized isoreticular compounds of the previously reported structures MIL-53, MIL-88B and MIL-101 (MIL = Matériaux Institute Lavoisier) by employing high-throughput synthetic methods.[27] Their study revealed that the insertion of functional groups in the organic linker can strongly change the synthesis conditions required for a desired structure. It was found that the nature of the reaction medium has the most profound impact on structure formation. Furthermore, the concentration of the starting mixture (*i.e.*, the solvent content) and the temperature were also identified as key parameters for the formation of the different competing hybrid phases. Building on our previous results on the structure-directed and oriented growth of the unfunctionalized MIL-88B crystals on carboxylate terminated SAMs,[28] we report here the direct growth of amino-functionalized oriented MILs on SAMs. The sorption behavior of these films was investigated using a quartz crystal microbalance (QCM).

Experimental

Preparation of self-assembled monolayers on gold

The gold-coated slides (glass slides (10 × 13 mm^2) coated with 10 nm Ti/100 nm Au by electron-beam evaporation, *Olympus AG*) were cleaned in ethanol and methanol. The cleaned gold slides were immersed in a 1 mM ethanolic solution (6 pieces in 30 mL) of 16-mercaptohexadecanoic acid (MHDA; 90%, *Aldrich*) and left at RT for 48 h. The SAM-functionalized gold slides were repeatedly washed with ethanol, and stored in fresh absolute ethanol until needed.

Synthesis of NH_2–Fe–MIL-88B

In a glass reactor, 1.00 g (5.52 mmol) of 2-amino-1,4-benzenedicarboxylic acid (99%, *Aldrich*) were dissolved in 15 mL dimethylformamide (DMF) (p.a., *Acros Organics*). The amount of 2.784 g (11.04 mmol) of $FeCl_3 \cdot 6H_2O$ (p.a., *Merck*) was added to the solution. The sealed-glass reactor was left for 24 h in a preheated oven at 150 °C. After cooling the synthesis mixture to room temperature, the crystalline product was filtered and stored for further characterization.

Preparation of the crystallization solution for film growth of NH_2–Fe–MIL-88B on –COOH terminated SAMs

In a 25 mL glass reactor, 0.25 g (1.4 mmol) of 2-amino-1,4-benzenedicarboxylic acid (99%, *Aldrich*) were dissolved in 15 mL dimethylformamide (DMF) (p.a., *Acros Organics*). The amount of 0.746 g (2.8 mmol) $FeCl_3 \cdot 6H_2O$ (p.a., *Merck*) and 1.38 mL of 1 M HCl was added to the clear solution. The sealed-glass reactor was left for 24 h in a preheated oven at 150 °C. After cooling the synthesis mixture to room temperature, the amorphous product was removed by filtration and the filtered solution was used for the growth of thin films.

Film-synthesis of NH_2–Fe–MIL-88B

The SAM-functionalized gold-slides were placed upside-down on Teflon®-supports into the filtered synthesis solution of NH_2–Fe–MIL-88B (3 pieces in 15 mL). The growth step took place at room temperature in a closed glass reactor. Immersion times were varied between 4 d and 11 d.

Synthesis of bulk NH_2–Fe–MIL-101 and preparation of the crystallization solution for film growth of NH_2–Fe–MIL-101

In a 25 mL glass reactor, 0.225 g (1.24 mmol) of 2-amino-1,4-benzenedicarboxylic acid (99%, *Aldrich*) were dissolved in 15 mL dimethylformamide (DMF) (p.a., *Acros Organics*). The amount of 0.675 g (2.5 mmol) $FeCl_3 \cdot 6H_2O$ (p.a., *Merck*) was added to the clear solution. The sealed glass reactor was left for 24 h in a preheated oven at 110 °C. After cooling the synthesis mixture to room temperature, the crystalline product was filtered off and stored for further characterization. The filtered solution was used for the growth of thin films.

Film growth of NH_2–Fe–MIL-101

The SAM-functionalized gold-slides were placed upside-down on Teflon®-supports into the filtered synthesis solution of NH_2–Fe–MIL-101 (3 pieces in 15 mL). The growth step took place at room temperature in a closed glass reactor. Immersion times were varied between 3 d and 10 d.

Characterization

X-Ray diffraction (XRD) measurements of powders were performed on a STOE powder diffractometer in transmission geometry (Cu-Kα_1, $\lambda = 1.5406$ Å), those of films using a Bruker D8 in θ–θ geometry (Cu-Kα_1, $\lambda = 1.5406$ Å; Cu-Kα_2, $\lambda = 1.5444$ Å).

A specially designed sample cell, the details of which are given in our previous publication[29] was used for the measurement of X-ray diffraction patterns under controlled partial pressures of a sorptive. The gas input in the lower part of the cell is connected to the flow-controlling system described in the ESI†. The cell was positioned onto the sample holder of a Scintag XDS 2000 X-ray diffractometer (Cu-Kα radiation, $\lambda = 1.54$ Å) measuring in θ–θ geometry. The powder patterns were recorded at angles between 5° and 35° 2θ with an interval of 0.01° 2θ and at a scan rate of 5° to 10° 2θ per minute.

Characterization of the self-assembled monolayers was performed by reflection absorption infrared (RAIR) spectroscopy, using a Bruker IFS 66v FTIR spectrometer. The sample chamber with a high performance variable angle reflection accessory (A-513) was maintained at 2 mbar during the entire measurement by means of an Edwards rotary-pump. In a typical measurement on gold surfaces, an angle of incidence of 83° to the surface normal was used. A cleaned gold slide was measured as background prior to the measurements. The morphology of the crystals was studied using a JEOL JSM-6500F scanning electron microscope.

Results and discussion

For the direct growth of the amino-functionalized MOF crystals, the gold substrates were modified with monolayers of HS $(CH_2)_{16}COOH$ following known procedures[30,31] (see Experimental section). The formation of the self-assembled monolayers was confirmed by RAIR, as shown in the ESI (Fig. S1†). The absorption band at 1554 cm^{-1}, characteristic for the presence of a carboxylate group, is indicated in the spectrum. The methylene groups of the aliphatic chains present high-frequency modes at 2920 and 2850 cm^{-1} associated with the asymmetric and symmetric C–H stretching vibrations, respectively; we also observe the band at 721 cm^{-1} assigned to the stretching vibration of the S–C bond.

Direct growth of NH_2–Fe–MIL-88B

Here we demonstrate the direct growth of an oriented amino-functionalized MOF, NH_2–Fe–MIL-88B on functionalized Au (111) substrates. The hexagonal 3D structure of NH_2–Fe–MIL-88B is built up from trimers of FeO_6 octahedra linked to benzenedicarboxylate anions. Thus the 3D pore system of MIL-88B consists of tunnels along the c axis connected by bipyramidal cages.[32] The structure of MIL-88B as well as the isoreticular amino-functionalized form is well known for their structural flexibility, which is reflected by large changes in their lattice parameters depending on the contents of the pores.[27,28,32–34]

In a previous study, we reported the oriented growth of Fe–MIL-88B crystals on self-assembled monolayers. The X-ray diffractograms of the crystals grown on the functionalized surface clearly exhibit [001] orientation, as only the 002 and the 004 reflections of Fe–MIL-88B are observed (Fig. 1, right).[28]

As shown in the XRD patterns of the synthesized film samples (depicted in Fig. 1 (left)), it was possible to obtain highly oriented films of NH_2–Fe–MIL-88B crystals on carboxylate-terminated self-assembled monolayers. As with the unfunctionalized Fe–MIL-88B structures, we obtained oriented growth in [001] direction. This can be seen by comparing the powder pattern of bulk NH_2–Fe–MIL-88B crystals with the diffraction patterns of the thin films of Fe–MIL-88B (Fig. 1).

The synthesis conditions for the first successful growth of NH_2–Fe–MIL-88B were determined starting from the synthesis of Fe–MIL-88B thin films and substituting the benzenedicarboxylic acid by 2-amino-benzenedicarboxylic acid. A second step of solvothermal treatment was found not to be necessary

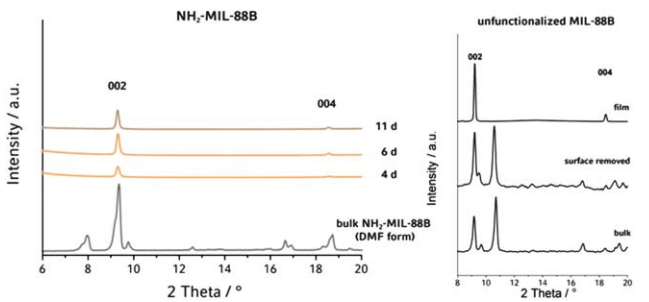

Fig. 1 Left: X-ray diffraction measurements of crystals grown on functionalized gold substrates compared to the XRD pattern of bulk NH_2–Fe–MIL-88B crystals. The immersion time of the substrates in the crystallization solution varied between 4 d and 11 d; right: XRD pattern of film on gold substrate (top), powder pattern of the removed crystals (center), and powder pattern of bulk Fe–MIL-88B (bottom).

because, contrary to the unfunctionalized system, precipitation of NH_2–Fe–MIL-88B at room temperature was already observed after one solvothermal step. However, the growth of NH_2–Fe–MIL-88B crystals was observed to be much slower than that of Fe–MIL-88B. This led us to investigate the effect of pH-variations of the crystallization solution on crystal growth. Different volumes of 1 M HCl were added to the initial reaction mixture, resulting in the formation of amorphous precipitation products during the post-solvothermal crystallization step at room temperature. The product of these reactions on the SAM-functionalized gold substrates is NH_2–Fe–MIL-88B. The X-ray diffraction patterns of directly grown NH_2–Fe–MIL-88B crystals on carboxylate terminated SAMs are presented in Fig. 2. Compared to the direct growth without addition of HCl, peak intensities of all samples from acidified batches are much more intense. We observe a maximum intensity for the 002 and the 004 reflections for a molar ratio of Fe^{3+} : HCl = 1 : 0.5. Despite this improved crystal growth on the surface, the bulk products of both precipitation steps, *i.e.* at 150 °C and at room temperature, are amorphous. Bauer *et al.* observed that addition of HCl led to the formation of mixtures of powders of NH_2–Fe–MIL-53 and NH_2–Fe–MIL-88B when water was used as the reaction medium. For DMF as the reaction medium, as in our case, the addition of NaOH favored the formation of NH_2–Fe–MIL-88B over the precipitation of NH_2–MIL-101. The addition of HCl to the synthesis in DMF is not mentioned in the study of Bauer *et al.* We can thus state that as the bulk product of the crystallization at room temperature is amorphous while NH_2–Fe–MIL-88B crystallizes on the functionalized substrates, we observe the catalysis of nucleation of NH_2–Fe–MIL-88B on the surface of the –COOH SAM. These terminal carboxyl groups of the SAM are presumed to mimic the functional groups of the NH_2–BDC ligand. Consequently, it is assumed that the terminal carboxylate groups of the SAM lead to a surface enrichment of metal ions and metal coordination allowing the subsequent attachment of the organic ligands. This interface-catalysed enrichment of the MOF building blocks is thought to enhance the nucleation rate of the MOF structure on the surface.

To further compare these results to our previous study on Fe–MIL-88B, SEM images were taken of the samples synthesized with and without addition of HCl (Fig. 3). It is obvious that direct growth of NH_2–Fe–MIL-88B takes place, even without addition of HCl. This can be seen from the magnified image in Fig. 3 (top). The XRD data shown in Fig. 1 also indicate that direct growth is occurring. However, even after longer immersion times of 11 d, only a few crystals have formed on the surface indicating that crystal growth had stopped at some point.

In contrast, the samples grown with addition of HCl show intergrowth of crystals and almost the complete sample surface is

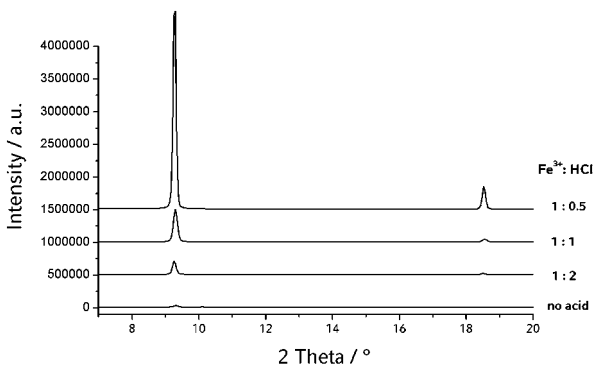

Fig. 2 X-Ray diffraction patterns of NH_2–Fe–MIL-88B thin films grown from crystallization solutions with different HCl content. The immersion time of the substrates in the crystallization solution was 11 d for all samples. Graphs are offset.

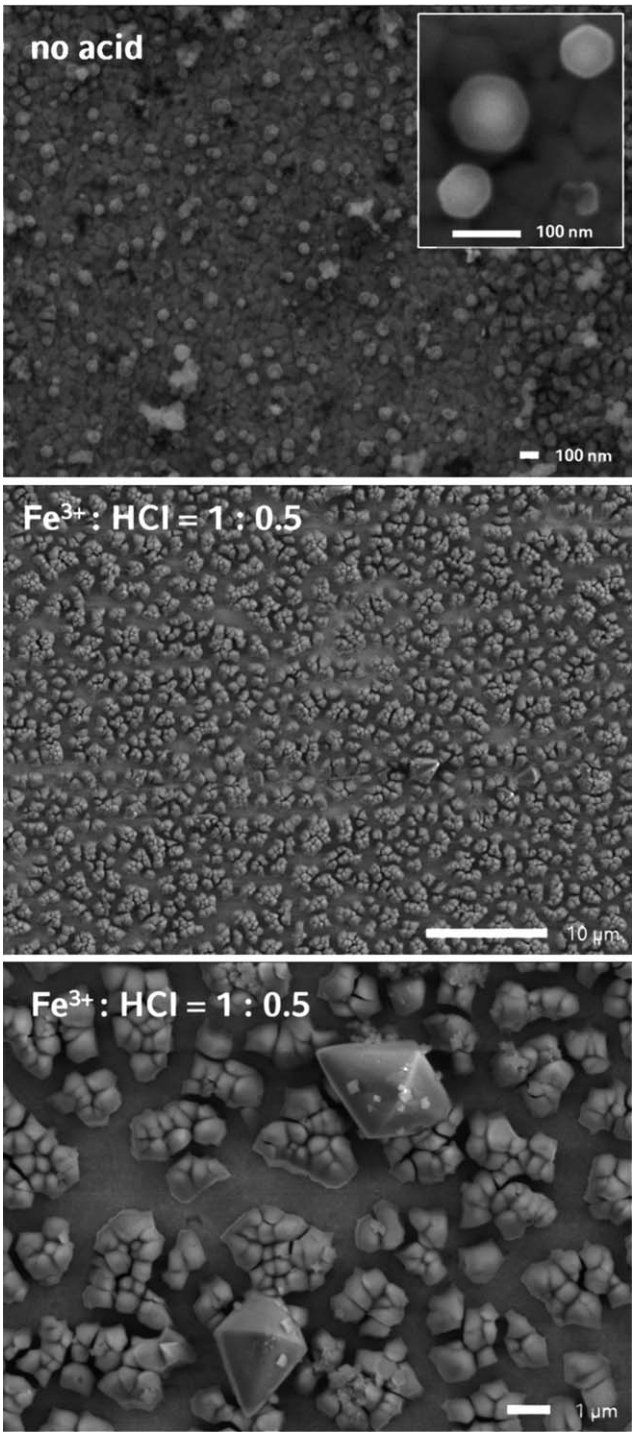

Fig. 3 Scanning electron micrographs of NH_2–Fe–MIL-88B crystals grown for 11 d on carboxylate terminated substrates.

covered. The cracks between the islands of crystals can be attributed to both the contraction of the flexible crystals during drying after synthesis in DMF as well as to shrinkage resulting from the ultra-high vacuum (UHV) in the SEM chamber. The homogeneity of the dense coatings is proven by optical light microscopy in addition to atomic force microscopy. The images clearly show that the cracks between the crystals are due to the UHV applied during scanning electron microscopy (see the ESI, Fig. S5 and S6†). In addition, further data on the MOF film thickness for differently prepared NH_2–Fe–MIL-88B batches are provided by scanning electron microscopy (see the ESI, Fig. S7†).

To study the differences between the functionalized and unfunctionalized Fe–MIL-88B films, sorption measurements with ethanol on a quartz crystal microbalance (QCM) were performed at room temperature. Fig. 4 represents the ethanol sorption isotherms of thin films of Fe–MIL-88B and NH_2–Fe–MIL-88B. Both isotherms show similar characteristic features. The first dosing step of ethanol leads to a steep increase in the amount adsorbed. At a relative pressure of ethanol of 0.16 there is another step in both isotherms. Both isotherms show hysteresis, however, this effect seems to be more pronounced for the amino-functionalized MOF films. The most remarkable difference between both isotherms is the total adsorbed amount. The adsorbed amount of ethanol recorded for the NH_2–Fe–MIL-88B crystals on the film at a relative pressure of ethanol of 0.16 is almost three times as high as that for the unfunctionalized films. At a relative pressure of 0.91 the amino-functionalized crystals adsorbed a total amount of 2.21 mmol g^{-1}, while the total adsorbed amount of the MIL-88B crystals is only 1.15 mmol g^{-1}.

The observed step in the isotherms and the differences in the adsorbed amount of ethanol raise the question as to whether these effects can be correlated to structural changes in the flexible MIL-88B structure.

To answer this question, the X-ray diffractograms of the film and powder samples of Fe–MIL-88B and of its isoreticular amino-functionalized analogue were recorded during the ad- and desorption of ethanol (sorption@XRD measurements). During the sorption@XRD measurements, which were performed at room temperature, the sorptive concentration in the flow was progressively increased, and then decreased. The results of the sorption@XRD measurements on thin films of Fe–MIL-88B with [001] orientation are depicted in Fig. 5a. The increase in the relative pressure of ethanol during adsorption evokes a shift in the 002 reflection to higher 2θ values, while during desorption the reflection shifts back towards low 2θ values. The related shifts for ethanol in the functionalized NH_2–Fe–MIL-88B are displayed in Fig. 5b.

The 002 reflection of oriented Fe–MIL-88B crystals shifts by about 0.08° 2θ during the adsorption in the sorption@XRD measurement, whereas the analogous shift for NH_2–Fe–MIL-88B is 0.15 2θ upon adsorption. Upon desorption from the unfunctionalized MOF, the 002 reflection shifts back to its original position, while the shift is not fully reversible with the amino-functionalized crystals. Importantly, these stepwise structural changes do not occur at the same partial pressures for the two MOF systems (see the ESI, Tables S1 and S2†).

As the XRD data from the oriented films only reveal structural changes in one crystallographic direction, the same sorption@XRD measurements were also performed on the corresponding powder samples, prepared as thin layers with random crystal orientation (Fig. 6 and 7).

In agreement with the experiments on the grown films, sorption@XRD measurements of the powder samples show a similar shift in the 002 reflection to smaller 2θ values for the functionalized and unfunctionalized crystals. As shown in Fig. 6, the complete diffraction pattern changes under a relative ethanol pressure of 0.02, compared to the pattern of the dried powder sample (p/p_0 0.00). During the following adsorption steps no further significant changes in the diffraction pattern are detected. This result is in good agreement with the QCM measurements (Fig. 4), where a steep increase in the amount adsorbed is shown for the first adsorption step, *i.e.* at p/p_0 0.02; and no large increase in the slope of the isotherm is observed for higher relative pressures. During desorption, the X-ray diffraction patterns show only small shifts in the reflections in the direction of their original position. Thus, under these conditions the small remaining amount of guest molecules is able to lock the structure of Fe–MIL-88B in its ethanolic form. Extended drying (N_2-flow: 100%) at room temperature removes all ethanol guest molecules from the pores (ESI, Fig. S2†).

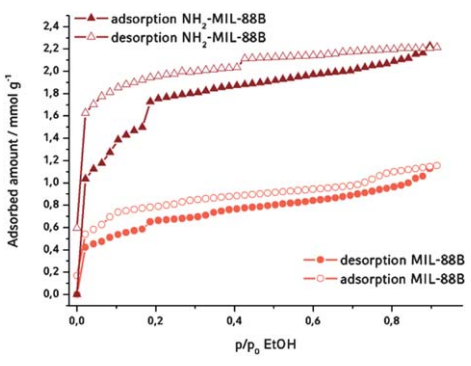

Fig. 4 Ethanol sorption isotherms of Fe–MIL-88B and NH_2–Fe–MIL-88B thin films, recorded with a quartz crystal microbalance at room temperature. The fact that the isotherms are not closing completely is attributed to very long equilibration times for the last desorption step.

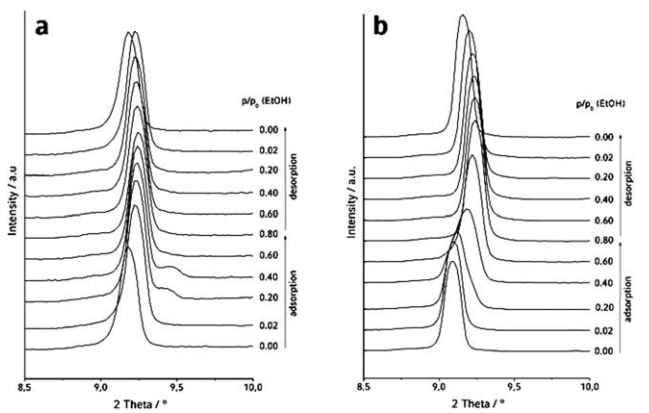

Fig. 5 (a) Shift in the 002 reflection of oriented Fe–MIL-88B and (b) NH_2–Fe–MIL-88B crystals on MHDA functionalized substrates upon ethanol adsorption and desorption.

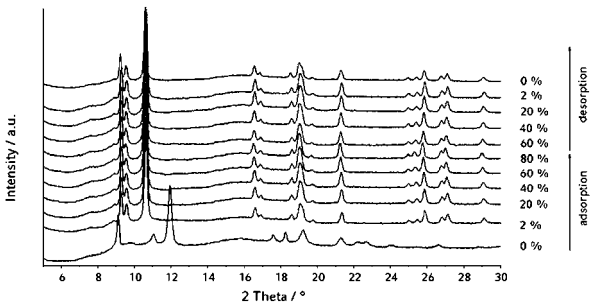

Fig. 6 X-Ray diffraction patterns of bulk Fe–MIL-88B prepared as a thin layer of randomly oriented crystals during the sorption@XRD measurement.

Fig. 7 shows the XRD data of the amino-functionalized NH_2–Fe–MIL-88B for various relative pressures of ethanol. In contrast to the unfunctionalized structure the diffraction patterns change remarkably during the first two dosing steps to p/p_0 0.02 and 0.2, respectively. Similar to the unfunctionalized system, beyond this pressure and upon desorption only small changes are observed. The structural changes at p/p_0 0.02 and 0.2 observed in the sorption@XRD measurements can be directly correlated to the steps in the sorption isotherm of NH_2–Fe–MIL-88B, which occur in the same partial pressure ranges.

Quantitative analysis of the structural changes in Fe–MIL-88B, based on the shift in 002, 100 and 101 reflection positions (Table 1), shows a significant increase in the unit cell volume by more than 500 Å^3 after the first dosing step, resulting from a decrease in c by about 0.4 Å and an increase in a by 1.4 Å. Similarly, for NH_2–Fe–MIL-88B the cell volume increases by about 500 Å^3 (decrease in c by 0.2 Å and increase in a by 1.4 Å). Both structures exhibit approximately the same increase in the cell volume during adsorption of ethanol. However, the total cell volume of NH_2–Fe–MIL-88B is slightly larger, which implies that the presence of the amino group causes a slight increase in the cell volume but does not influence the flexibility of the structure (Table 2).

Summarizing, the structural changes in these flexible frameworks observed upon adsorption are fairly similar and cannot explain the much higher uptake of ethanol of the amino-functionalized host, as revealed by the QCM experiments. We therefore attribute the strong difference in sorption behavior to the incorporated amino functionality within the pores of NH_2–Fe–MIL-88B. It is proposed that significant host–guest interactions such as hydrogen bonding cause the larger adsorbed amount of ethanol at a defined relative pressure. Similar observations supporting this interpretation have been recently made in computational studies.[35] The authors were able to demonstrate the significant impact of ligand functionalization on CO_2 and CH_4 adsorption loading. The calculated isotherms show a considerable enhancement in the CO_2 uptake with respect to the original form of the MOF. The increased adsorption is asserted to result from additional interactions such as hydrogen bonding.

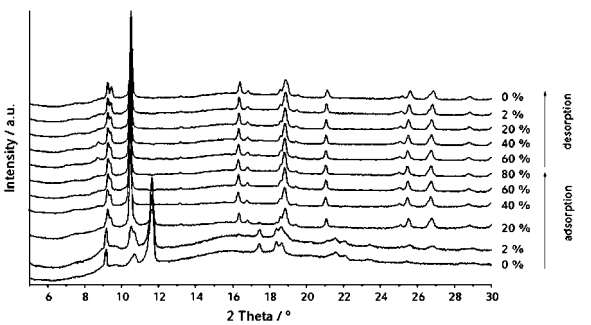

Fig. 7 X-Ray diffraction patterns of bulk NH_2–Fe–MIL-88B showing the shift in the reflection positions of a thin layer of randomly oriented crystals during the sorption@XRD measurement.

Table 1 Lattice parameters a and c of Fe–MIL-88B after indexing using the Werner algorithm for different relative pressures of ethanol

p/p_0	Lattice parameter a/Å	Lattice parameter c/Å	Cell volume/Å^3
0.00	9.3	19.4	1662
0.02	10.7	19.1	2167
0.40	10.7	19.0	2175
0.80	10.7	19.0	2184

Table 2 Lattice parameters a and c of NH_2–Fe–MIL-88B after indexing using the Werner algorithm for different relative pressures of ethanol

p/p_0	Lattice parameter a/Å	Lattice parameter c/Å	Cell volume/Å^3
0.00	9.5	19.3	1756
0.02	10.6	19.3	2180
0.40	10.9	19.1	2250
0.80	10.9	19.1	2260

Direct growth of oriented NH_2–Fe–MIL-101 on a self-assembled monolayer

The direct growth methodology was also extended to the synthesis of thin films of NH_2–Fe–MIL-101 on carboxylate-terminated self-assembled monolayers. The intriguing properties

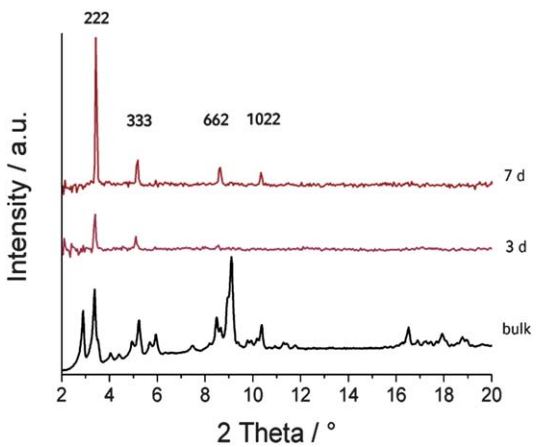

Fig. 8 X-Ray diffraction data of NH_2–Fe–MIL-101 crystals grown on functionalized gold substrates (immersion times of the substrates in the crystallization solution of 3 d and 7 d) compared to the powder pattern of bulk NH_2–Fe–MIL-101 crystals. The background of the XRD patterns of the film samples was subtracted.

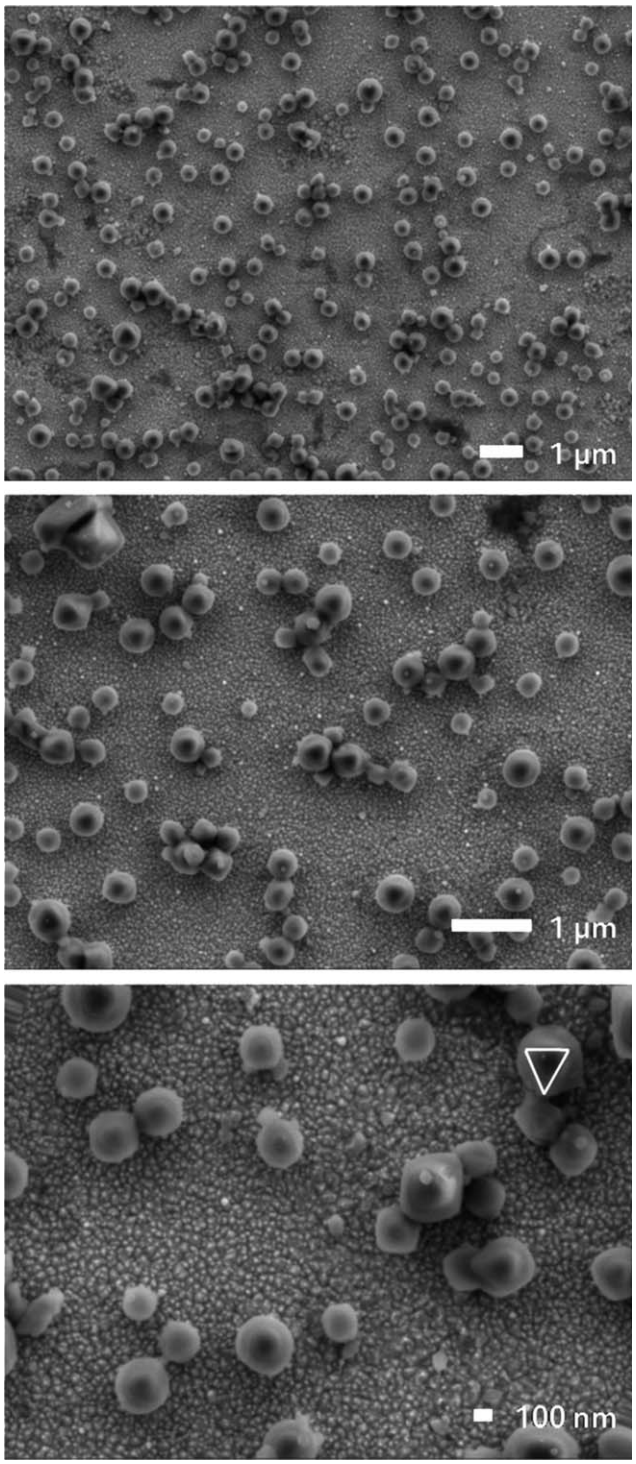

Fig. 9 Scanning electron micrographs of NH_2–Fe–MIL-101 samples after immersion time of 10 d, at different magnifications.

of bulk NH_2–Fe–MIL-101 are demonstrated by thermogravimetric analysis (TGA) and nitrogen sorption data; the results are depicted in Fig. S3 and S4 (ESI†). The crystallization solution used in this synthesis was prepared in the same way as the synthesis solution for bulk NH_2–Fe–MIL-101.[27] NH_2–Fe–MIL-101 is isoreticular to MIL-101, which has a cubic unit cell with a cell parameter of 89 Å. After an immersion time of 3 d, the 222 reflection at 3.4° 2θ and the 333 reflection at 5.1° 2θ of NH_2–Fe–MIL-101 can be clearly detected (Fig. 8). The increase in the immersion time to 7 d leads to a strong increase in the intensities of the 222 and 333 reflections. Small additional reflections at 8.6° and 10.3° 2θ (662 and 1022 reflections of NH_2–Fe–MIL-101), indicate the appearance of a few additional less oriented crystals. We conclude that the crystal populations on the SAM have a strongly preferred orientation in the [111]-direction.

Scanning electron microscopy (SEM) of the films shows crystals with a distinct sphere-like morphology with sizes between 100 and 500 nm (Fig. 9). Higher magnification reveals that most of the crystals have a triangular top-face (Fig. 9, bottom), in good agreement with the preferred [111]-orientation of the crystals deduced from the XRD results. NH_2–Fe–MIL-101 crystallizes in a cubic symmetry and the bulk crystals show an octahedral morphology, which would appear with triangular habit viewed in the [111] direction.

Conclusions

In this study, we have shown that functionalized metal–organic frameworks can be grown on self-assembled monolayers and that a preferred orientation of the crystals can be achieved. This was demonstrated for the flexible structure of NH_2–Fe–MIL-88B as well as the large cage structure of NH_2–Fe–MIL-101. The influence of the implemented functionality on the sorption properties of MIL-88B compared to its modified analogue was investigated by QCM experiments. A considerably enhanced uptake of ethanol was demonstrated for the amino-functionalized MOF. We attribute this impact of ligand modification to secondary interactions such as hydrogen bonding with the guest molecules. Moreover, a correlation of the adsorbed amount of ethanol with structural changes in the flexible Fe–MIL-88B systems was observed *in situ* by sorption@XRD measurements. Our study shows that the concept of oriented crystal growth on SAM-modified gold substrates can be extended to functionalized porous structures. The growth method apparently can be generalized to an increasing number of MOF structures, such that comparative sorption experiments in thin films become possible.

We anticipate that the ability to direct the growth of functionalized MOFs in the form of thin oriented films will be of particular interest in applications such as selective chemical sensors, where both the control of crystal growth orientation and functionalization of the organic linker are expected to have a strong impact on sensitivity, kinetics and selectivity through specific host–guest interactions.

Acknowledgements

Financial assistance from DFG (SPP 1362) is gratefully acknowledged. J. J. Williams would like to thank the Royal Academy of Engineering for a Global Researcher Award through which this work was undertaken. The authors thank Bastian Rühle for assistance with SEM and AFM data acquisition as well as graphics design.

Notes and references

1 A. K. Cheetham, C. N. R. Rao and R. K. Feller, *Chem. Commun.*, 2006, 4780–4795.

2 A. U. Czaja, N. Trukhan and U. Mueller, *Chem. Soc. Rev.*, 2009, **38**, 1284–1293.
3 S. Bauer and N. Stock, *Chem. Unserer Zeit*, 2008, **42**, 12–19.
4 G. Ferey and C. Serre, *Chem. Soc. Rev.*, 2009, **38**, 1380–1399.
5 D. J. Tranchemontagne, J. L. Mendoza-Cortes, M. O'Keeffe and O. M. Yaghi, *Chem. Soc. Rev.*, 2009, **38**, 1257–1283.
6 D. Zacher, O. Shekhah, C. Woell and R. A. Fischer, *Chem. Soc. Rev.*, 2009, **38**, 1418–1429.
7 C. Munuera, O. Shekhah, H. Wang, C. Woell and C. Ocal, *Phys. Chem. Chem. Phys.*, 2008, **10**, 7257–7261.
8 O. Shekhah, H. Wang, T. Strunskus, P. Cyganik, D. Zacher, R. Fischer and C. Woell, *Langmuir*, 2007, **23**, 7440–7442.
9 O. Shekhah, H. Wang, S. Kowarik, F. Schreiber, M. Paulus, M. Tolan, C. Sternemann, F. Evers, D. Zacher, R. A. Fischer and C. Woell, *J. Am. Chem. Soc.*, 2007, **129**, 15118–15119.
10 O. Shekhah, H. Wang, D. Zacher, R. A. Fischer and C. Woell, *Angew. Chem., Int. Ed.*, 2009, **48**, 5038–5041, S5038/5031–S5038/5033.
11 D. Zacher, A. Baunemann, S. Hermes and R. A. Fischer, *J. Mater. Chem.*, 2007, **17**, 2785–2792.
12 S. Hermes, D. Zacher, A. Baunemann, C. Woell and R. A. Fischer, *Chem. Mater.*, 2007, **19**, 2168–2173.
13 S. Hermes, F. Schroeder, R. Chelmowski, C. Woell and R. A. Fischer, *J. Am. Chem. Soc.*, 2005, **127**, 13744–13745.
14 E. Biemmi, C. Scherb and T. Bein, *J. Am. Chem. Soc.*, 2007, **129**, 8054–8055.
15 N. S. John, C. Scherb, M. Shoeaee, M. W. Anderson, M. P. Attfield and T. Bein, *Chem. Commun.*, 2009, 6294–6296.
16 O. M. Yaghi, M. O'Keeffe, N. W. Ockwig, H. K. Chae, M. Eddaoudi and J. Kim, *Nature*, 2003, **423**, 705–714.
17 S. Kitagawa, S.-I. Noro and T. Nakamura, *Chem. Commun.*, 2006, 701–707.
18 S. Kitagawa and K. Uemura, *Chem. Soc. Rev.*, 2005, **34**, 109–119.
19 Z. Wang and S. M. Cohen, *Chem. Soc. Rev.*, 2009, **38**, 1315–1329.
20 Y.-F. Song and L. Cronin, *Angew. Chem., Int. Ed.*, 2008, **47**, 4635–4637.
21 J. S. Seo, D. Whang, H. Lee, S. I. Jun, J. Oh, Y. J. Jeon and K. Kim, *Nature*, 2000, **404**, 982–986.
22 A. D. Burrows, C. Frost, M. F. Mahon and C. Richardson, *Angew. Chem., Int. Ed.*, 2008, **47**, 8482–8486.
23 K. K. Tanabe, Z. Wang and S. M. Cohen, *J. Am. Chem. Soc.*, 2008, **130**, 8508–8517.
24 Z. Wang and S. M. Cohen, *J. Am. Chem. Soc.*, 2007, **129**, 12368–12369.
25 Z. Wang and S. M. Cohen, *Angew. Chem., Int. Ed.*, 2008, **47**, 4699–4702.
26 M. J. Ingleson, J. P. Barrio, J.-B. Guilbaud, Y. Z. Khimyak and M. J. Rosseinsky, *Chem. Commun.*, 2008, 2680–2682.
27 S. Bauer, C. Serre, T. Devic, P. Horcajada, J. Marrot, G. Ferey and N. Stock, *Inorg. Chem.*, 2008, **47**, 7568–7576.
28 C. Scherb, A. Schoedel and T. Bein, *Angew. Chem., Int. Ed.*, 2008, **47**, 5777–5779.
29 C. Scherb, R. Koehn and T. Bein, *J. Mater. Chem.*, 2010, **20**, 3046–3051.
30 A. Ulman, *Chem. Rev.*, 1996, **96**, 1533–1554.
31 H. Wang, S. Chen, L. Li and S. Jiang, *Langmuir*, 2005, **21**, 2633–2636.
32 S. Surble, C. Serre, C. Mellot-Draznieks, F. Millange and G. Ferey, *Chem. Commun.*, 2006, 284–286.
33 C. Serre, C. Mellot-Draznieks, S. Surble, N. Audebrand, Y. Filinchuk and G. Ferey, *Science*, 2007, **315**, 1828–1831.
34 C. Mellot-Draznieks, C. Serre, S. Surble, N. Audebrand and G. Ferey, *J. Am. Chem. Soc.*, 2005, **127**, 16273–16278.
35 A. Torrisi, R. G. Bell and C. Mellot-Draznieks, *Cryst. Growth Des.*, 2010, **10**, 2839–2841.